ORIGINAL RESEARCH

Serelaxin Improves Regional Myocardial Function in Experimental Heart Failure: An In Vivo Cardiac Magnetic Resonance Study

Tomas Lapinskas, MD;* Sebastian Kelle, MD;* Jana Grune, PhD;* Anna Foryst-Ludwig, PhD; Heike Meyborg, BSc; Sarah Jeuthe, PhD; Ernst Wellnhofer, MD; Ahmed Elsanhoury, BSc; Burkert Pieske, MD; Rolf Gebker, MD; Ulrich Kintscher, MD; Philipp Stawowy, MD

***Background*—**Animal studies demonstrated that serelaxin lessens fibrosis in heart failure. This study assessed its effect on myocardial deformation using cardiac magnetic resonance and elucidated its relationship to gene regulation and histology in a mouse heart failure model.

***Methods and Results*—**C57BL/6J mice were subjected to SHAM (n=4) or transverse aortic constriction (TAC). At week 10, TAC mice were randomized to receive either serelaxin (0.5 mg/kg per day; n=11) or vehicle (n=13) for 4 weeks. Cardiac magnetic resonance imaging was performed at baseline and repeated at the end of the study (week 14). Cine images were used to calculate left ventricular (LV) global longitudinal, circumferential, and radial strain. Hearts were examined for histology and gene expression. Compared with SHAM, mice 10 weeks after TAC showed increased LV mass with significant decreases in LV deformation parameters, indicating subclinical deterioration of myocardial function. At week 14, TAC mice given serelaxin demonstrated significant improvements in all LV strain parameters and no decrease in LV stroke volume and ejection fraction compared with TAC mice given vehicle. A significant positive correlation between global circumferential strain and the extent of myocardial fibrosis was found, and global circumferential strain correlated significantly with the expression of heart failure genes in serelaxin-treated mice.

***Conclusions*—**Serelaxin improved cardiac magnetic resonance–derived myocardial deformation parameters as well as histomorphometric and gene expression findings in mice with heart failure. Cardiac magnetic resonance–derived myocardial mechanics correlate with histology and gene expression, stressing its utilization in myocardial remodeling. **(*J Am Heart Assoc*. 2020;9:e013702. DOI: 10.1161/JAHA.119.013702.)**

Key Words: cardiac magnetic resonance • feature tracking • heart failure • myocardial fibrosis • serelaxin

Heart failure (HF) is a leading cause of hospitalization and mortality in patients older than 65 years and its prevalence is expected to increase within the next decades.[1] Despite significant improvement in the care of chronic HF, treatment of acute HF (AHF) remains challenging, with a 30-day readmission rate of ≈1 quarter, thus also having an enormous impact on patients' quality of life and productivity.[2]

Based on left ventricular (LV) dysfunction, patients are classified as having HF with reduced ejection fraction or HF with preserved ejection fraction, both carrying a similar poor prognosis.[3,4] Generally, when admitted with AHF, the majority of patients present with dyspnea, renal impairment, and a normal to elevated systolic blood pressure.[5] AHF pathophysiology is multifaceted, comprising default systolic and diastolic ventricular function and myocardial injury, vascular and renal dysfunction, and an inflammatory and neurohormonal response.[6] Treatment of AHF typically combines the use of vasodilators and diuretics with the addition of inotropic agents in patients with hypotension, usually leading to rapid decongestion and symptom relief. However, this is likely incomplete as the disease is characterized by a downward spiral of progression with an overall poor prognosis.[7] Thus, a number of new drugs have been introduced for AHF treatment.

In the RELAX-AHF (Serelaxin, Recombinant Human Relaxin-2, for Treatment of Acute Heart Failure) study, patients with AHF were randomized to receive either serelaxin (n=581) or placebo (n=580) in addition to standard of care for the initial 48 hours

From the Department of Medicine/Cardiology, Deutsches Herzzentrum Berlin, Berlin, Germany (T.L., S.K., J.G., H.M., S.J., E.W., A.E., B.P., R.G., P.S.); Department of Cardiology, Medical Academy, Lithuanian University of Health Sciences, Kaunas, Lithuania (T.L.); DZHK (German Center for Cardiovascular Research), Partner Site Berlin, Berlin, Germany (S.K., J.G., A.F.-L., S.J., B.P., R.G., U.K., P.S.); Department of Cardiology, Virchow Clinic (S.K., A.E., B.P.) and Center for Cardiovascular Research and Institute of Pharmacology (J.G., A.F.-L., U.K.), Charité-Universitätsmedizin Berlin, Berlin, Germany.

*Dr Lapinskas, Dr Kelle, and Dr Grune contributed equally to this work.

Correspondence to: Philipp Stawowy, MD, Department of Medicine/Cardiology, Deutsches Herzzentrum Berlin, Augustenburger Platz 1, 13353 Berlin, Germany. E-mail: stawowy@dhzb.de

Received June 21, 2019; accepted December 6, 2019.

Clinical Perspective

What Is New?

- Using serelaxin in a rodent heart failure model and in a therapeutic setting, we found that the improvement of myocardial cardiac magnetic resonance deformation parameters by serelaxin parallels and correlates with changes in myocardial histology and gene expression.

What Are the Clinical Implications?

- Cardiac magnetic resonance tissue tracking techniques are sensitive to quantify early changes in myocardial deformation parameters and reflect changes in histology and gene expression.
- Applying these novel imaging biomarkers will affect patient treatment and clinical outcome.

after admission.[8] Serelaxin treatment resulted in significant symptomatic improvement and reduced the hospital stay and worsening of HF through day 5, which was associated with improvement in biomarkers. Furthermore, serelaxin resulted in a statistically significant 37% reduction in both cardiovascular death and all-cause mortality through day 180 compared with placebo.[8] However, the more recent RELAX-AHF-2 trial, could not replicate mortality benefits in 3274 serelaxin-treated patients with acute decompensated HF compared with placebo (n=3271).[9]

Molecularly, serelaxin has antifibrotic and anti-inflammatory actions, which are mediated via ligation to its cognate G protein–coupled receptor RXFP1 (relaxin/insulin-like family peptide receptor 1), expressed throughout the cardiovascular system.[10] Signal transduction involves pathways including cAMP, NO, endothelin B, and transforming growth factor-β (TGF-β)/Smad 2/3.[10] In spontaneous hypertensive rats, serelaxin treatment improves cardiac and renal fibrosis, involving the inhibition of cardiac fibroblast proliferation and myofibroblast differentiation and the aberrant collagen deposition.[11]

The present study aimed to further elucidate the impact of serelaxin on pressure overload–induced HF in mice in a therapeutic scenario. For this, we utilized a complementary and comparative approach of molecular biology and cardiac magnetic resonance (CMR) feature tracking (CMR-FT), which offers the advantage to quantitatively investigate cardiac performance beyond LV ejection fraction (LVEF) and other standard functional parameters by high-resolution techniques, comparing findings to histology and gene expression in a well-defined, reproducible animal model.

Methods

The authors declare that all supporting data are available within the article.

Animal Model

Eight- to 9-week-old male C57BL/6J mice (weight 22–25 g) were randomized to transverse aortic constriction (TAC, n=35) or SHAM (n=5) surgery. During the study period, 12 mice were lost to animal welfare, with 4 SHAM and 24 TAC mice completing the study (Figure 1). Mice were housed at 12 hours light/dark cycle in a temperature-controlled animal facility and fed normal chow ad libitum. Briefly, surgery mice were anesthetized by intraperitoneal injection of ketamine/xylazine (80 ng/mL; 12 mg/mL per kg of body weight [BW]), and a partial thoracotomy to the second rib was performed. The thymus was gently separated, and adipose tissue was dissected from the aortic arch. Aortic ligation was performed between the innominate and left common carotid artery, using a 6.0 silk suture placed around a 26G needle. SHAM mice underwent the identical procedure except aortic ligation. After surgery, mice received flunixin (2.5 mg/kg SC). At week 10, TAC-operated mice were randomized to receive either serelaxin (0.5 mg/kg per day, provided by Novartis; TAC_Srlxn [n=11]) or the equivalent volume of vehicle (sodium acetate, pH 5.0; TAC_Veh [n=13]) continuously via ALZET minipumps (DURECT Corporation) over the next 4 weeks. SHAM mice were neither treated with serelaxin or vehicle because our previous studies demonstrated that SHAM-operated mice do not develop any significant changes in myocardial deformation parameters assessed by CMR.[12] In accordance, SHAM mice did not develop LV hypertrophy at week 4 on echocardiography in this study. All animal procedures were performed in accordance with the guidelines of the German Law on the Protection of Animals, and the state office review committee approved the protocol (G0099/14).

Echocardiography

Echocardiography was performed 1 week before and 4 weeks after surgery using a high-resolution digital imaging platform (Vevo 3100 Imaging System, VisualSonics, Inc) equipped with a high-frequency transducer (MX400 with frequency range of 18–38 MHz and axial resolution of 50 μm). Mice were anesthetized with isoflurane-oxygen (3%) and continuously monitored by ECG. The interventricular septum and LV posterior wall thickness and LV end-diastolic diameter were used to determine LV mass and LVEF. LV mass was calculated from M-mode images according to the Penn-cube formula.[13]

Cardiac Magnetic Resonance

CMR images were acquired using a 3.0 Tesla small animal magnetic resonance imaging system (MRS 3017, MR Solutions) with a quadrature birdcage cardiac volume coil. After induction of inhalation anesthesia using isoflurane-oxygen (4–

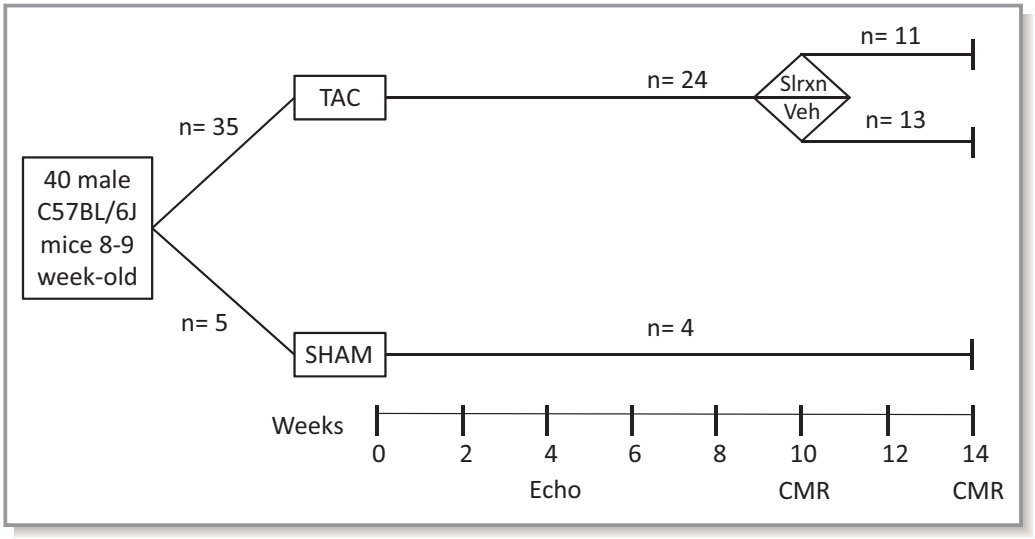

Figure 1. Experimental design and number of mice assigned to each group and number of mice completing the study. CMR indicates cardiac magnetic resonance; Slrxn, serelaxin; TAC, transverse aortic constriction; Veh, vehicle.

5%), animals were placed on a dedicated mouse sledge and magnetic resonance imaging–compatible ECG electrodes were attached to the paws. Anesthesia was maintained with isoflurane-oxygen (1.5–2%) to adjust heart rate at 400 to 450 beats per minute. The study protocol included initial scouts to determine cardiac imaging planes. Images were acquired using respiratory and ECG-gated gradient-echo cine sequences in 2- and 4-chamber long-axis planes and stacks of 5 to 7 short-axis slices completely covering the entire left ventricle. Typical image parameters were 15 phases per cardiac cycle, repetition time=10 ms, echo time=3 ms, averages=4, field of view=40×40 mm, pixel size=0.15×0.15 mm, and slice thickness=1 mm.

Images were analyzed using commercially available software CMR[42] (Circle Cardiovascular Imaging Inc). LV end-diastolic and end-systolic volumes were quantified using manual planimetry of the endocardial and epicardial surface from short-axis stack, and LV stroke volume and LVEF were calculated.

Cine images were used to calculate LV myocardial strain using the same software. Endocardial and epicardial contours were manually drawn in both long-axis and 3 short-axis (at basal, midventricular, and apical levels) views at end-diastole for each mouse. After application of a tracking algorithm, the software automatically identified myocardial borders throughout the cardiac cycle and computed segmental and global myocardial strain values. LV global longitudinal strain (GLS) was calculated be averaging the strain curves of both 2- and 4-chamber long-axis views. LV global circumferential (GCS) and radial strain (GRS) were derived by averaging the strain curves of basal, midventricular, and apical short-axis views. All images were analyzed 3 times and derived measurements were averaged.

Histology and Histomorphometry

Hearts were formalin-fixed, paraffin-embedded, and stained with hematoxylin and eosin. Picrosirius red staining was performed according to the manufacturer's protocol. Periarteriolar fibrosis was measured as percentage of stained collagen areas (magnification ×40) with 5 randomly chosen high-power fields analyzed. Cardiomyocyte sizes were analyzed as described by measuring 20 cardiomyocytes in at least 3 randomly chosen areas (magnification ×20).[14]

Immunoblotting

For Western blot analysis, heart tissue samples from SHAM, TAC_Veh, and TAC_Srlxn mice (n=3 separate mice from each group) were lysed in radioimmunoprecipitation assay buffer (50 mmol/L Tris pH 7.5, 150 mmol/L NaCl, 5 mmol/L $MgCl_2$, 1% Nonidet P-40, 2.5% glycerol, 1 mmol/L EGTA, 50 mmol/L NaF, 1 mmol/L Na_3VO_4, 10 mmol/L $Na_4P_2O_7$, 100 µmol/L phenylmethylsulfonyl fluoride) and complete protease/phosphatase inhibitor cocktail (PhosSTOP and Complete Mini, Roche Diagnostics) with Lysis Tube P (Biometra, Analytik Jena) and SpeedMill system (Analytik Jena). Immunoblotting was performed as previously described using the following antibodies: collagen-type 3α1 (Col3A1) (sc28888, Santa Cruz), matrix metalloproteinase (MMP)-2 (sc-10736, Santa Cruz), TGFbeta (ab 92486, Abcam), tissue inhibitor of metalloproteinase (TIMP)-3 (sc 30075, Santa

Cruz), and GAPDH (Abcam), and secondary horseradish-conjugated antibodies (Jackson ImmunoResearch Inc).[15] For detection, enhanced chemiluminescent reagents (ECL kit, Thermo Scientific) were used and densitometry was performed with ChemiDoc (BioRad) according to the manufacturer's instructions and the data were then expressed as ratio (percentage).

Serelaxin Serum Levels

Blood samples collected in heparin tubes were centrifuged at 1000*g* (15 minutes) and supernatants snap frozen at −80°C. The Human Relaxin-2 ELISA Kit (DRL200, R&D Systems) was used according to the manufacturer's protocol. Measurements were performed with a microplate reader cap (absorbance at 450 nm), with a correction wavelength set at 540 nm or 570 nm. Duplicates of standards and samples were averaged, and the averaged zero standard optical density was subtracted afterwards. Software analysis CurveExpert 3.1 was used for curve fit analysis.

Gene Expression Analysis

Heart tissue was immediately snap frozen and stored at −80°C. Sample preparation, microarray procedure of RT² Profiler PCR Array (Qiagen), and analysis followed the manufacturer's instructions. Briefly, total RNA was isolated from liquid nitrogen–frozen left ventricles with the RNeasy Micro Kit. cDNA was synthesized by using the RT² PreAMP cDNA Synthesis Kit. Subsequently, samples were used to perform an RT² Profiler PCR Array, focusing on genes associated with fibrosis. Results were analyzed using the provided web-based RT² Profiler PCR Array Data Analysis version 3.5. Relative abundance of mRNA was calculated after normalization to a reference gene panel consisting of ACTB (β actin), B2M (β2-microglobulin), GADPH, GUSB (glucuronidase β), and HSP90AB1 (heat shock protein 90 alpha family class B member 1).

Quantitative Real-Time PCR

Heart samples (10 mg) were homogenized and used for quantitative real-time polymerase chain reaction (PCR) in SHAM (n=4), TAC_Veh (n=6), and TAC_Srlxn (n=6) mice. Briefly, total RNA was isolated with the RNeasy Micro Kit (Qiagen), according to the manufacturer and total RNA amount was measured using a spectrophotometer (NanoDrop). RNA (1 μg) was reverse transcribed using reverse transcriptase, RNAsin, and dNTPs (Promega), and used in quantitative PCR in the presence of a fluorescent dye (Sybrgreen). Internal controls lacking reverse transcriptase were prepared and measured in parallel. Relative abundance of mRNA was calculated after normalization to the reference gene murine 18S with the 2-ddct method. Measurements were performed in technical triplicates and were accompanied by using nontemplate controls (UP-H_2O) as internal controls. Primer sequences were used as follows (100 nmol/L): murine 18s (for: 5′-TTAATGAGCCATTCGCAGTTTTC-3′, Rev: 5′-ACCTGGTTGATCCTGCCAGTAG-3′), murine natriuretic peptide type B (for: 5′-CACCGCTGGGAGGTCACT-3′, Rev: 5′-GTGAGGCCTTGGTCCTTCAA-3′), murine β-myosin heavy chain (β-MHC; for: 5′-TTCCTTACTTGCTACCCTC-3′, Rev: 5′-CTTCTCAGACTTCCGCAG-3′), murine CD68 (for: 5′-ACTGGTGTAGCCTAGCTGGT-3′, Rev: 5′-CCTTGGGCTATAAGCGGTCC-3′), murine relaxin/insulin-like family peptide receptor 1 (for: 5′- GATCTGAAGGAGCTGTCGCA-3′, Rev: 5′-CTGAGAGACTTGAGTTTGGC-3′), and murine actin (for: 5′-GACAGGATGCAGAAGGAGATTACTG-3`, Rev: 5′-GCTGATCCACATCTGCTGGAA-3′).

Statistical Analysis

While calculating the sample size of the study, we assumed a Wilcoxon-Mann-Whitney test for the difference of means with a power of 80% and an α of 0.05. The allocation ratio for testing of LV hypertrophy in TAC versus SHAM animals was chosen as 7 in order to have a large group of TAC animals suitable for subgrouping in a treatment and nontreatment (vehicle) group with an allocation ratio of 1. With an allocation ratio of 7, about 26 animals would be enough to test large effects of serelaxin on LV hypertrophy. Assuming a dropout rate of 25%, the total necessary sample size was 40 animals. The sample size calculation was performed using G*Power, version 3.1.9.4.[16] Data are expressed as mean±SD or median and range in case of data without normal distribution. Differences were assessed by parametric (*t* test, ANOVA, repeated measurements model) and nonparametric (Kruskal–Wallis) tests using SPSS version 23 (IBM). A *P* value of <0.05 was regarded as significant. Post hoc correction for multiple comparisons was performed according to Tukey. Box plots were constructed using R and RStudio with the package foreign importing the SPSS data.

Results

Transverse Aortic Banding Leads to Compensated Hypertrophy in Mice

Male C57BL/6J mice (n=40) were randomly assigned to receive either SHAM (n=5) or TAC (n=35) surgery, with 4 SHAM and 24 TAC mice completing the study (Figure 1). To confirm successful aortic banding, echocardiography was performed at week 4. Analysis demonstrated the presence of significant LV hypertrophy in TAC mice (interventricular septum thickness at end-diastole: 0.79±0.05 cm; LV mass/

BW: 3.85±0.41) compared with SHAM mice (interventricular septum thickness at end-diastole: 0.54±0.04 cm; LV mass/BW: 2.75±0.22 in SHAM [both $P<0.001$]) (Figure 2A and 2B). However, despite the presence of a high transaortic pressure gradient (maximal gradient 32.34±13.56 mm Hg), TAC-operated animals did not show a significant reduction in LVEF when compared with SHAM-operated mice (Figure 2C).

At week 10, TAC-operated mice were randomized to receive either serelaxin (0.5 mg/kg per day; TAC_Srlxn [n=11]) or the equivalent volume of vehicle (TAC_Veh, n=13) continuously over the next 4 weeks. SHAM-operated mice (n=4) were also included (Figure 1). At baseline, mice underwent CMR examination for the assessment of basic volumetric/functional parameters, as well as analysis of regional LV myocardial performance (Figure 3). Compared with SHAM control, TAC mice displayed significant decreases in GCS and GRS, with GLS being nonsignificantly reduced and without alterations in LV stroke volume and LVEF (Table 1).

Serelaxin Reduced Cardiac Fibrosis and Hypertrophy in Mice With Transverse Aortic Banding

At the end of the 4-week serelaxin treatment (week 14 after surgery) all mice underwent end point CMR imaging. Animals were than euthanized and serum and organs harvested. Serum analysis demonstrated that TAC-operated, serelaxin-treated mice had several-fold higher serelaxin serum levels when compared with TAC_Veh or SHAM mice ($P<0.001$). No difference in serelaxin serum levels was found between SHAM and TAC_Veh mice (Figure 4A). Immunohistochemical and histomorphometric analysis of cardiac cross-sections from the midventricular level demonstrated areas of fibrosis mostly localized to periarteriolar regions (Figure 4B). While SHAM mice displayed little fibrosis (2.37±0.75 μm^2), it was increased in TAC_Veh mice (7.38±3.65 μm^2, $P=0.023$ versus SHAM). Serelaxin treatment significantly reduced cardiac fibrosis (3.76±1.81 μm^2, $P=0.013$ versus TAC_Veh), restoring it to levels present in SHAM mice (P=NS versus SHAM) (Figure 4C). Reduction of TAC-mediated fibrosis by serelaxin was accompanied by a significant decrease in cardiomyocyte size used as an index of hypertrophy. In TAC_Veh mice, cardiomyocyte size significantly increased compared with that in the SHAM mice (18.46±1.32 μm^2 TAC_Veh versus 16.25±0.86 μm^2 SHAM, $P=0.015$). These changes were reversed in TAC_Srlxn mice (17.30±1.41 μm^2, P=NS versus SHAM) (Figure 4D).

Serelaxin Improved Cardiac Function During HF Transition

The end point CMR demonstrated that over the 14 weeks following surgery, TAC_Veh mice advanced from LV hypertrophy with preserved LVEF to HF (Figure 5A and 5B). This was apparent by a significantly depressed LVEF (45.22±7.76% at end point CMR versus 51.73±7.11% baseline CMR, $P=0.006$) and a reduced LV stroke volume (16.76±4.87 mL at end point CMR versus 21.54±5.64 mL baseline CMR, $P=0.039$) in TAC_Veh mice as compared with baseline. In contrast, deterioration of LVEF was prevented in TAC_Srlxn mice (50.07±6.48% at end point versus 49.78±9.34% at baseline CMR, $P=0.799$). In addition, LV

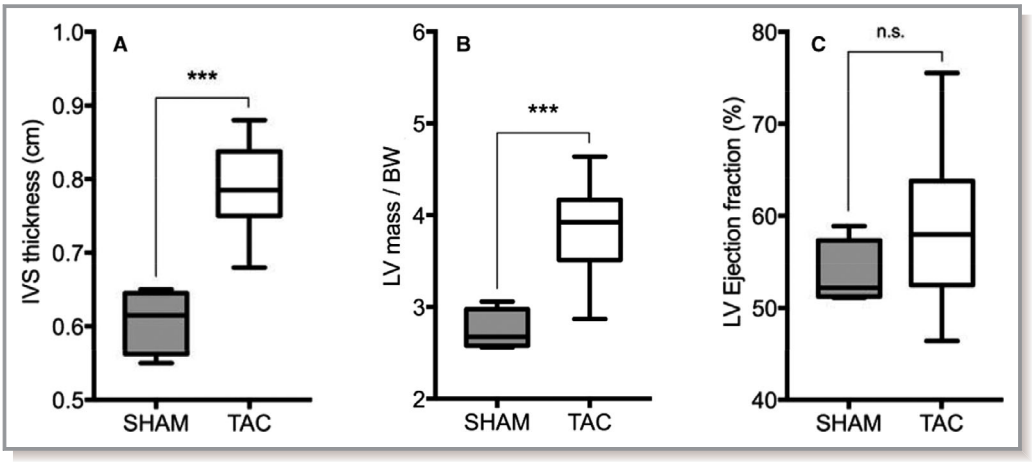

Figure 2. Comparison of left ventricular (LV) morphological and functional parameters between SHAM- and transverse aortic constriction (TAC)–operated mice derived using M-mode echocardiography 4 weeks after surgery. Estimated thickness of interventricular septum (IVS) (**A**) and calculated LV mass (**B**) were significantly higher in TAC mice (***$P<0.001$). There was no significant reduction in left ventricular ejection fraction (LVEF) (**C**) between SHAM- and TAC-operated mice ($P=0.209$). BW indicates body weight.

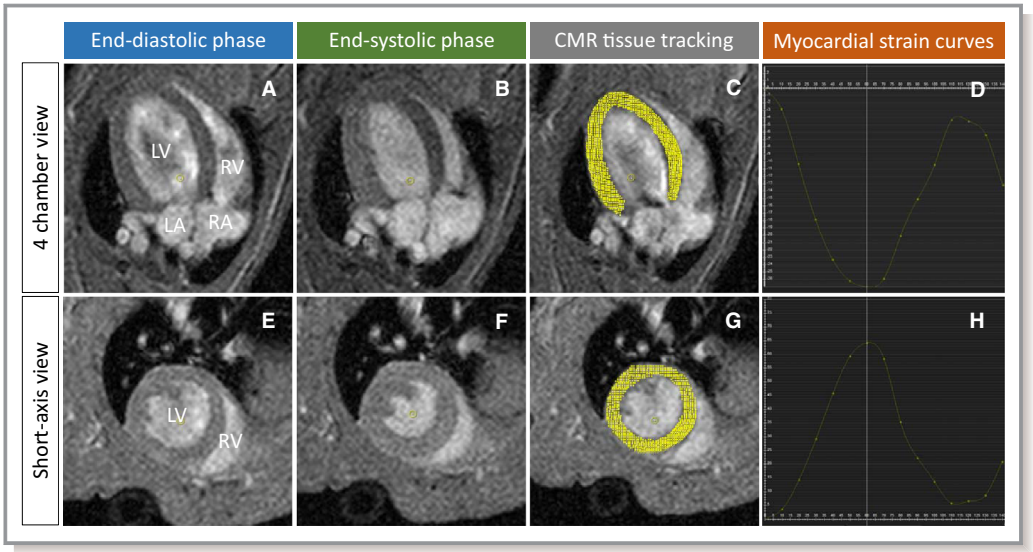

Figure 3. Cine cardiac magnetic resonance (CMR) images without and with endocardial and epicardial contouring and examples of CMR feature tracking myocardial global strain curves in mice. An end-diastolic frame from cine images of the long-axis 4-chamber (**A**) and short-axis at midventricular level (**E**) as well as end-systolic frame from cine images of the long-axis 4-chamber (**B**) and short-axis at midventricular level (**F**) demonstrate all cardiac chambers. Cine images of the long-axis 4-chamber (**C**) and short-axis at midventricular level (**G**) after manual contouring and automatic endocardial and epicardial border detection during entire cardiac cycle. An example of left ventricular (LV) global longitudinal (**D**) and LV global radial (**H**) strain curves derived from long-axis and short-axis cine images, respectively. LA, left atrium; LV, left ventricle; RA, right atrium; RV, right ventricle.

stroke volume was significantly depressed in TAC_Veh mice after 14 weeks compared with that in TAC_Srlxn mice (Figure 5A and 5B). All animals also underwent morphometric analysis (Table 2). Comparison of groups demonstrated a significant difference in heart weight (HW), as well as HW normalized to either tibia length (HW/tibia length) or BW (HW/BW) between SHAM and TAC_Veh mice, as well as SHAM and TAC_Srlxn mice. However, no significant difference was found when comparing TAC_Veh with TAC_Srlxn mice (Table 2).

Table 1. Comparison of CMR Parameters at Week 10

	SHAM (n=4)	TAC (n=24)	*P* Values
Volumetric parameters			
LVSV, mL	30.46±7.26	21.69±5.70	0.144
LVEF, %	71.28±8.20	50.82±8.01	0.144
Myocardial deformation parameters			
LVGLS, %	−20.35±3.07	−16.07±4.18	0.082
LVGCS, %	−20.65±4.02	−15.89±3.10	0.015
LVGRS, %	45.24±11.47	29.56±7.52	0.012

Results are expressed as mean±SD. CMR indicates cardiac magnetic resonance; LVEF, left ventricular ejection fraction; LVGCS, left ventricular global circumferential strain; LVGLS, left ventricular global longitudinal strain; LVGRS, left ventricular global radial strain; LVSV, left ventricular stroke volume; TAC, transverse aortic constriction.

Serelaxin Improved Myocardial Mechanics Correlate With Changes in Gene Expression

Analysis of myocardial strain by CMR-FT showed that TAC_Srlxn mice had significant improvement in LV GLS (−13.95±3.50% at baseline versus −17.53±1.98% at end point, *P*=0.007), GCS (−14.78±2.80% at baseline versus −17.49±2.09% at end point, *P*=0.001), and GRS (27.42±7.52% at baseline versus 34.46±7.34% at end point, *P*=0.006). In contrast, there was a significant deterioration of LV GCS (−16.71±3.30% at baseline versus −14.16±2.00% at end point, *P*=0.023) and GRS (30.83±7.81% at baseline versus 26.25±5.18% at end point, *P*=0.028) in TAC_Veh mice. Likewise, analysis of percentage change of regional myocardial function between groups demonstrated a significant difference between TAC_Srlxn and TAC_Veh for all parameters investigated (Figure 5C through 5E). Accordingly, a significant difference in GCS and GRS was evident between TAC_Srlxn and SHAM mice, in which strain did not change over the time course.

A gene array was used as a screening tool to investigate whether changes in myocardial deformation parameters are escorted by changes in gene expression (Figure 6A). Analysis of clustergrams demonstrates that serelaxin treatment impacted genes involved in extracellular matrix remodeling and cell motility. Thus, serelaxin increased MMP-2, -3, and -14, while decreasing their tissue inhibitors of MMPs (TIMP-2, -3, and -4).

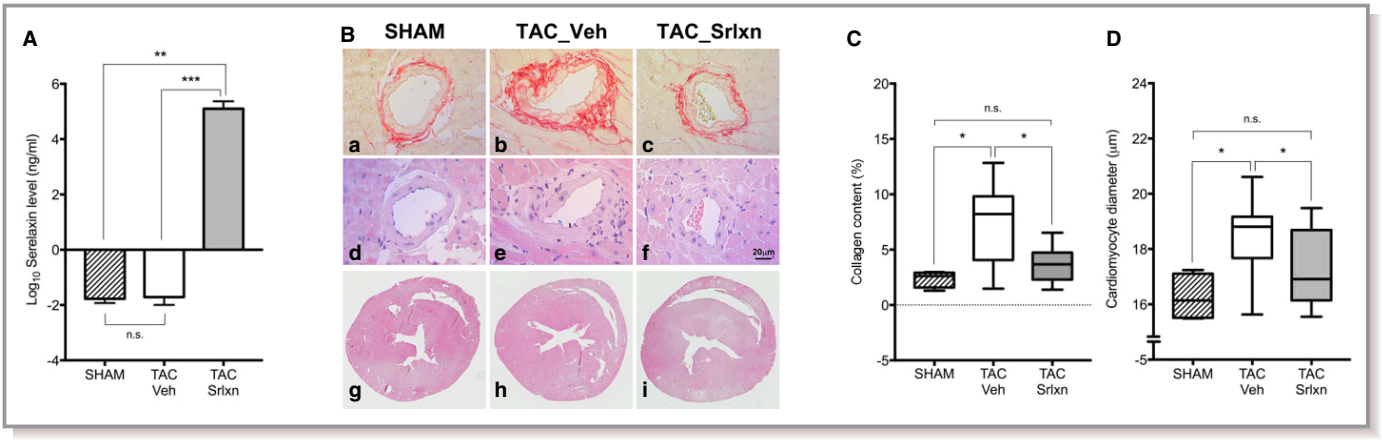

Figure 4. (**A**) Comparison of serelaxin serum levels in all 3 study groups demonstrated that serelaxin levels were several-fold higher in transverse aortic constriction (TAC) mice given serelaxin (TAC_Srlxn) when compared with both vehicle (TAC_Veh) (***P<0.001) and SHAM mice (**P<0.01). No difference in serelaxin levels was found between SHAM and TAC_Veh mice (P=0.684). (**B**) Immunohistochemistry showed that compared to SHAM mice periarteriolar fibrosis was increased in TAC_Veh mice, whereas serelaxin treatment of TAC mice (TAC_Srlxn) resulted in less fibrosis (a-c = Picrosirius red staining; d-f = hematoxylin/eosin staining; g-i = cardiac cross sections at midventricular level). (**C**) TAC_Srlxn mice demonstrated significantly less collagen content when compared with TAC_Veh mice (*P<0.05). (**D**) Similarly, cardiomyocytes size was significantly decreased in TAC_Srlxn mice compared to TAC_Veh mice (*P<0.05).

This was accompanied by increases in collagens (eg, type-1α2). Likewise, integrins (eg, integrin α1 and αv), important for cell/cell and cell/matrix communication, were induced by serelaxin. In contrast, members of the TGF-β/Smad 2/3 signaling cascade were downregulated. To investigate fibrosis-associated protein regulation, Western blot experiments were performed with heart samples from individual animals from each group. Immunoblotting demonstrated that the balance between the MMP inhibitor TIMP-3 and MMP-2 was significantly altered in TAC_Srlxn mice compared with SHAM and TAC_Veh mice (Figure 6B upper panel and Figure 6C, data expressed as ratio TIMP-3/MMP-2; SHAM=0.904±0.201, TAC_Veh=0.952±0.300, TAC_Srlxn=0.461±0.117 [±SD]; SHAM versus TAC_Veh: P=NS, SHAM versus TAC_Srlxn: P<0.05 and TAC_Veh versus TAC_Srlxn: P<0.05). This was accompanied by a decreased protein expression of TGF-β and Col3α1 (Figure 6B, lower panel).

o quantify a differential gene regulation between groups, we performed additional quantitative real-time PCR analysis of selected genes in LV samples from SHAM, TAC_Veh, and TAC_Srlxn mice. As our study demonstrates, β-MHC mRNA (SHAM: 1.025±0.275; TAC_Veh 11.175±3.258; TAC_Srlxn: 5.298±1.972 [±SD]) and BNP (B-type natriuretic peptide) mRNA (SHAM: 1.033±0.302; TAC_Veh: 3.055±0.183; TAC_Srlxn: 2.098±1.647 [±SD]), used as markers of LV hypertrophy and HF, were strongly upregulated in TAC_Veh mice and significantly decreased by serelaxin (Figure 6D and 6E). However, CD68 mRNA (SHAM: 1.013±0.156; TAC_Veh: 0.940±0.289; TAC_Srlxn: 0.770±0.140 [±SD]) used as an indicator of inflammation or RXFP1 (SHAM: 1.07±0.39; TAC_Veh: 1.78±1.62; TAC_Srlxn: 2.80±1.69 [±SD]) itself were not significantly regulated between groups (Figure 6F and 6G).

Last, we aimed to investigate whether serelaxin treatment of TAC mice corresponds and correlates with changes of histology and genes, as well as alterations in CMR deformation parameters (Figure 7A through 7F). Ultimately, our data demonstrate that serelaxin treatment is associated with lesser fibrosis and accompanied by serelaxin-induced gene regulation (ie, downregulation of BNP and β-MHC mRNA levels in TAC_Srlxn mice). Consequently, serelaxin treatment was also complemented by significant changes in regional myocardial function, apparent by a higher GCS in TAC_Srlxn mice. Thus, regional myocardial deformation (strain) regulated by serelaxin, corresponds and correlates with changes in histology and gene expression.

Discussion

The present study demonstrates that serelaxin prevents further deterioration and leads to an improvement of global and regional myocardial deformation parameters assed by high-resolution CMR in mice with pressure-overload HF. The aim of this study was to prove beneficial actions of serelaxin in advanced HF disease progression, thus its administration was postponed until imaging demonstrated compensated cardiac failure. Over the course of this study, LVEF and functional parameters deteriorated in untreated TAC mice. Hence, serelaxin prevented a further decrease in LV stroke volume and LVEF, accompanied by a significant improvement in myocardial mechanics assed by CMR-FT in TAC mice. Ultrastructural and molecularly, serelaxin led to a decrease in

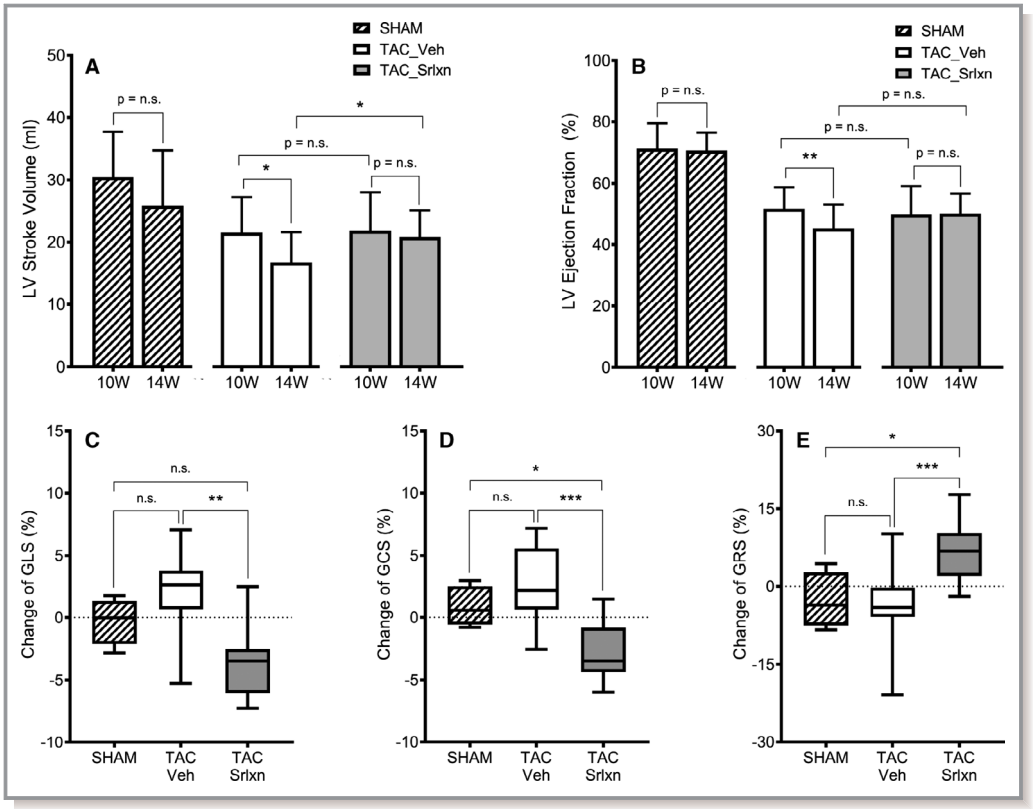

Figure 5. Comparison of left ventricular (LV) functional parameters derived at baseline (week 10) and end point (week 14). Cardiac magnetic resonance studies demonstrated that transverse aortic constriction (TAC) mice given vehicle (TAC_Veh) developed significant reduction in LV stroke volume (**A**) (**P*<0.05) and LV ejection fraction (LVEF) (**B**) (***P*<0.01). However, this was not found in TAC mice given serelaxin (TAC_Srlxn) mice. There was significant improvement in global longitudinal strain (GLS) (**C**), global circumferential strain (GCS) (**D**), and global radial strain (GRS) (**E**) after 4 weeks of treatment in TAC_Srlxn mice, compared with TAC_Veh (***P*<0.01 for GLS; ****P*<0.001 for GCS and GRS) or SHAM (**P*<0.05) mice.

periarteriolar fibrosis and a halt in cardiomyocyte hypertrophy, accompanied by regulation of genes key to cardiac remodeling.

In TAC-operated rodents, aortic constriction rapidly leads to pressure-induced cardiomyocyte hypertrophy followed by increases in LV mass and later on deterioration in LV

Table 2. Comparison of Postmortem Cardiac and Pulmonary Remodeling

Parameter	SHAM (n=4)	TAC_Veh (n=13)	TAC_Srlxn (n=11)	*P* Values		
				(SHAM vs TAC_Veh)	SHAM vs TAC_Srlxn)	TAC_Veh vs TAC_Srlxn)
HW, g	0.14±0.01	0.17±0.02	0.17±0.04	0.003**	0.026*	0.277
LW, g	0.16±0.03	0.17±0.02	0.16±0.02	0.871	0.851	0.186
BW, g	29.15±0.91	28.63±1.93	29.05±2.64	0.703	0.851	0.820
TL, mm	16.98±0.06	17.13±0.08	16.91±0.40	0.262	0.489	0.134
HW/BW, mg/g	4.91±0.43	6.05±0.46	6.02±1.34	0.003**	0.026*	0.167
HW/TL, mg/mm	8.41±0.55	10.26±1.05	10.30±2.19	0.002**	0.010*	0.190
LW/BW, mg/g	5.61±0.89	5.82±0.71	5.39±0.63	0.703	0.571	0.228
LW/TL, mg/mm	9.63±1.50	9.77±1.23	9.19±0.85	0.862	0.851	0.235

Results are expressed as mean±SD. BW indicates body weight; HW, heart weight; HW/BW, heart weight to body weight ratio; HW/TL, heart weight to tibia length ratio; LW, lung weight; LW/BW, lung weight to body weight ratio; LW/TL, lung weight to tibia length ratio; TAC_Srlxn, transverse aortic constriction mice given serelaxin; TAC_Veh; transverse aortic constriction mice given vehicle; TL, tibia length.
**P*<0.05.
***P*<0.005).

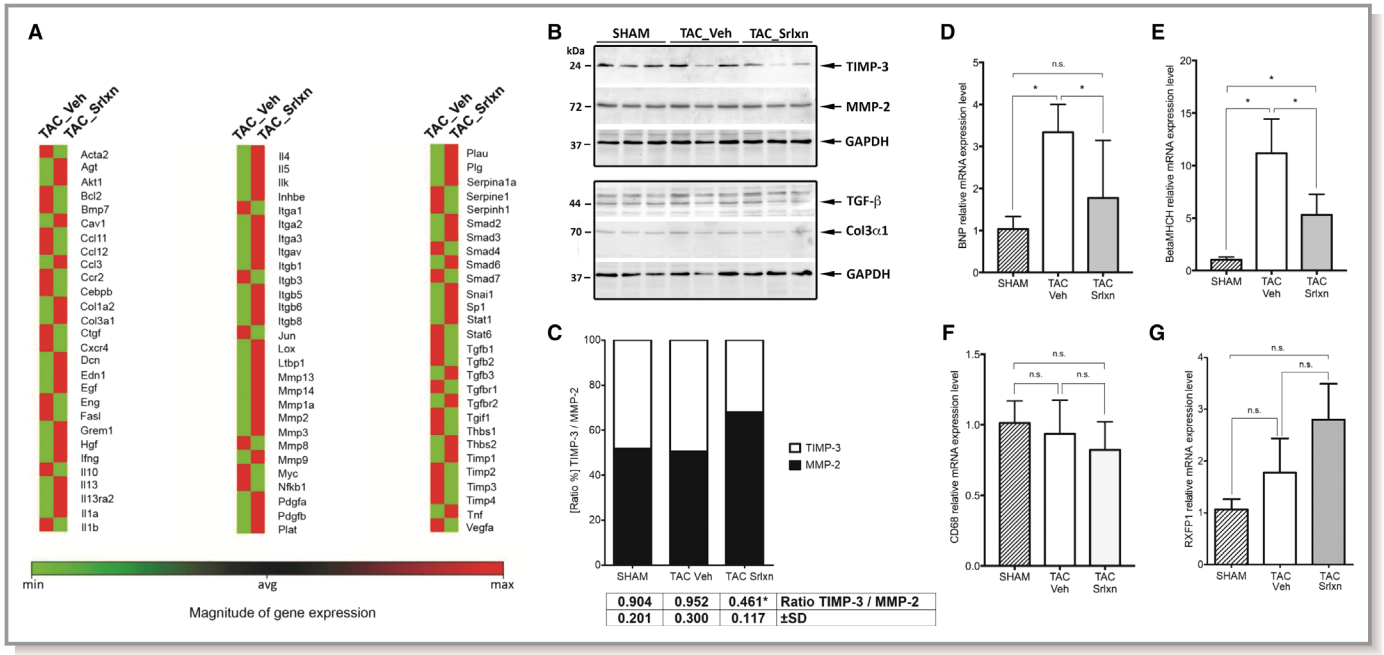

Figure 6. Gene expression profiling of left ventricular (LV) samples from transverse aortic constriction (TAC) mice given vehicle (TAC_Veh) and TAC mice given serelaxin (TAC_Srlxn) mice. **A**, Data assessed by an 82-gene polymerase chain reaction (PCR)–based microarray focusing on fibrosis depicted in clustergrams (n=3 per group). A panel of housekeeping genes, including GADPH, GUSB, and Hsp90ab1 was incorporated. **B**, Immunoblotting demonstrated that the balance between the matrix metalloproteinase (MMP) inhibitor tissue inhibitor of metalloproteinase (TIMP)-3 and MMP-2 was significantly altered in TAC_Srlxn mice compared with SHAM and TAC_Veh mice (**B** upper panel). **C**, Demonstrates the expression ratio of TIMP-3/MMP-2 in murine cardiac tissue samples, n=3 separate mice from each group; SHAM vs TAC_Veh: *P*=NS, SHAM vs TAC_Srlxn and TAC_Veh vs TAC_Srlxn: **P*<0.05. This was accompanied by a decreased protein expression of transforming growth factor-β (TGF-β) and collagen type-3α1 (Col3α1) (**B**, lower panel). GAPDH demonstrates protein loading. **D**, BNP (B-type natriuretic peptide) mRNA (SHAM: 1.033±0.302; TAC_Veh: 3.055±0.183; TAC_Srlxn: 2.098±1.647 [±SD]) was significantly upregulated in TAC_Veh mice in the quantitative PCR analysis. This was prevented by serelaxin treatment (TAC_Srlxn) (**P*<0.05). **E**, Comparable results were found when investigating β-myosin heavy chain mRNA (SHAM: 1.025±0.275; TAC_Veh 11.175±3.258; TAC_Srlxn: 5.298±1.972 [±SD]) (**P*<0.005), whereas no significant changes in CD68 gene expression (**F**) (SHAM: 1.013±0.156; TAC_Veh: 0.940±0.289; TAC_Srlxn: 0.770±0.140 [±SD]) (*P*<NS) or RXFP1 (relaxin/insulin-like family peptide receptor 1) mRNA (**G**) (SHAM: 1.07±0.39; TAC_Veh: 1.78±1.62; TAC_Srlxn: 2.80±1.69 [±SD]) (*P*<NS) were found (n=3–6 per group).

performance leading to HF.[17] Gene expression analysis demonstrated that this is associated with a rapid (within hours) regulation of embryogenic genes, such as natriuretic peptide precursor type A, myosin heavy chain-β, or α-skeletal actin.[18,19] Further downstream signaling pathways such as TGF-β/Smad 2/3 and ERK1/2 MAP-kinases participate, affecting fibroblast proliferation and fibrosis.[20] Using a quantitative PCR array for screening, we found that serelaxin differentially affected key regulators of cardiac fibrosis, including the balance between collagen-degrading MMPs and their TIMP inhibitors (eg, MMP-2, -9, -13 and TIMP-2 and -4), the collagens (eg, Col 1α2), and the intracellular regulators of TGF-β signaling (eg, Smad 2/3). Western blot analysis from heart samples was used to further investigate the protein levels of fibrosis and matrix remodeling–associated genes. We show that the balance in protein expression between TIMP-3/MMP-2 is decreased in serelaxin-treated TAC-operated mice, likely affecting gelatinolytic activities.[21] In addition to its effect on cardiac fibroblast differentiation and proliferation, relaxin has been shown to lessen collagen content and collagen deposition.[22] Likewise, our immunoblotting experiments demonstrate downregulation of TGF-β and Col-3α1 upon serelaxin-treatment of TAC-operated mice. Furthermore, quantitative real-time PCR demonstrated significant downregulation of the TAC-induced cardiac hypertrophy genes β-MHC and BNP in serelaxin-treated mice, escorted by decreases in fibrosis and hypertrophy on histology.

In vitro serelaxin has been shown to inhibit TGF-β–induced rat cardiac fibroblast differentiation, their proliferation/migration, as well as their MMP/TIMP ratios and collagen overproduction involving activin receptor-like kinase 5/Smad 2/3 pathways.[23] Administration of serelaxin to serelaxin $^{-/-}$ or β_2-adrenergic receptor transgenic mice reduced cardiac collagen content as well as MMP expression and collagen overproduction from isolated cardiac fibroblast.[22] Whereas short-term (3 day) serelaxin administration had mainly beneficial vascular effects in the angiotensin II/N(ω)-nitro-L-arginine methyl ester chronic HF mice model, continuous

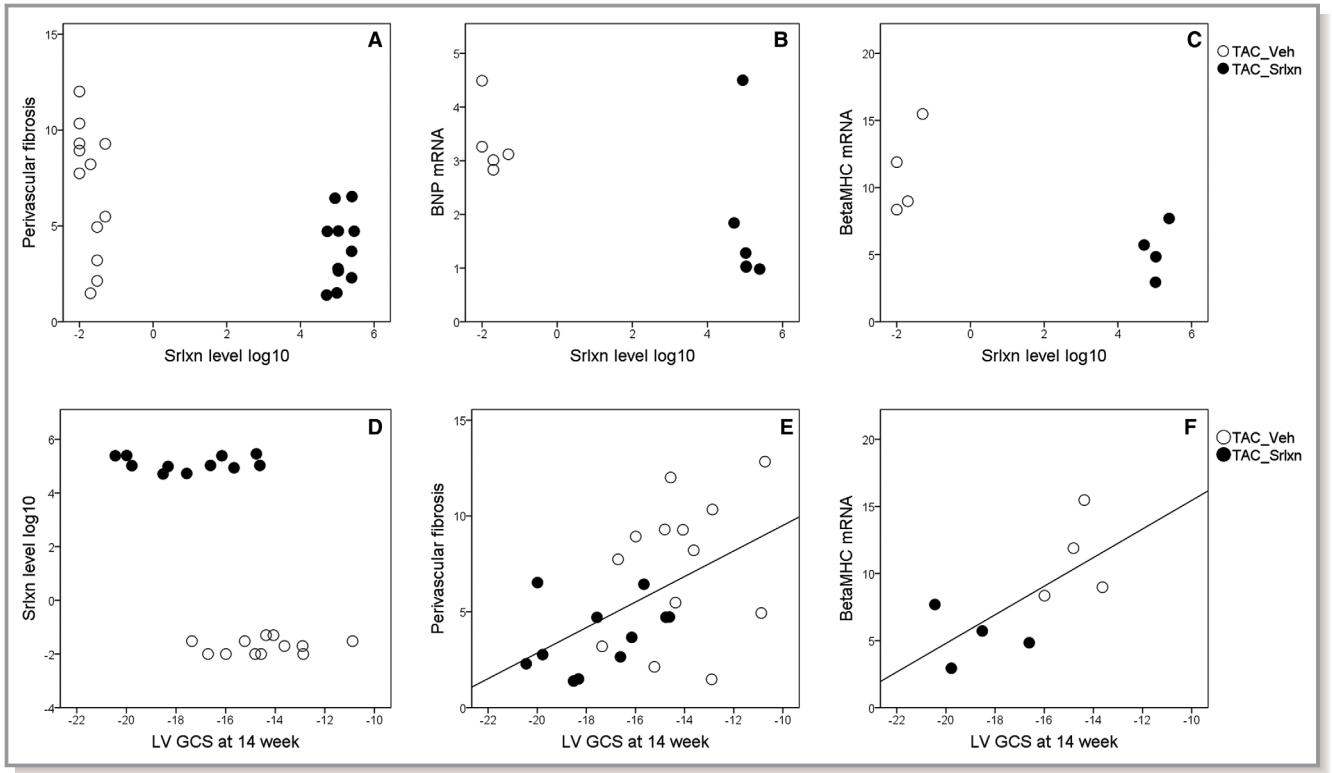

Figure 7. Upper panel: association and correlation analysis between serelaxin (Srlxn) serum levels and the presence of left ventricular (LV) fibrosis (**A**), levels of BNP (B-type natriuretic peptide) mRNA (**B**), and β-myosin heavy chain (β-MHC) (**C**). Lower panels: association and correlation analysis between left ventricular circumferential strain (GCS) and Srlxn serum levels (**D**), fibrosis (**E**), and β-MHC mRNA expression (**F**).

serelaxin administration (4 weeks) in DOCA-salt rats inhibited cardiac hypertrophy assed by echocardiography, associated with an attenuation of bone morphogenetic protein and β-MHC mRNA expression.[24,25] In contrast, despite an improvement in renal inflammation and fibrosis following long-term serelaxin treatment, no effect on echocardiographic parameters was found in mice with dilated cardiomyopathy.[26] These differences might be attributable to factors such as the animal model, mice strain, time/length of serelaxin administration, and imagine technique used.

Early deterioration of myocardial deformation parameters assessed by tissue tracking techniques are sensitive markers of the failing myocardium and precede detectable changes in LVEF, clinical cardiac impairment, and overt HF.[27] Clinically, myocardial deformation parameters have been demonstrated as independent predictors of mortality in patients with HF.[27–30] The recently introduced CMR-FT method has provided additional insights in HF pathophysiology and risk stratification, as well as understanding the myocardial adaptation to treatment.[30–33] CMR-FT myocardial deformation imaging is a new technique that allows quantification of myocardial motion and strain using routine cine images by tracking the actual endocardial and epicardial borders over time. Recently, myocardial deformation imaging has been applied in small animal studies.[34] Hence, cardiac remodeling has been investigated in TAC-operated C57BL/6 mice longitudinally (weekly, 1–13 weeks) by CMR.[35] Mice were divided into "mild" TAC (aortic arch tied off by a 25G needle) and "severe" TCA (27G needle) groups.[35] "Severe" TAC mice displayed a rapid decline in cardiac parameters and increase in HW/tibia length and pulmonary remodeling, but also had a higher mortality.[35] In the present study, we used a 26G needle leading to an "intermediate" TAC phenotype without pulmonary remodeling and randomized mice to serelaxin or vehicle treatment when CMR-FT demonstrated subclinical abnormalities in myocardial contractility, indicating the transition to decompensated HF. In addition to improvements in volumetric and anatomical parameters (eg, LVEF and histology), serelaxin significantly impacted myocardial deformation parameters in TAC mice. Thus, using CMR-FT for the assessment of LV myocardial function beyond the evaluation of LVEF, we show that in TAC mice, serelaxin significantly improved GLS, GCS, and GRS and attenuated decreases in LV stroke volume and LVEF compared with vehicle treatment. In contrast, van Nierop et al[35] did not find differences in radial wall thickening or circumferential wall shorting between control and "mild" TAC mice, but differences in the extent of TAC as a result of mice strain and surgery might contribute.[36]

Still comparable to our study, the authors found a significantly decreased radial wall thickening and circumferential wall shortening in their "severe" TAC mice.[35]

Echocardiography has been used to investigate myocardial deformation in small animals. In murine myocardial infarction, high-frequency speckle tracking echocardiography–derived strain parameters were significantly reduced, correlating with LV mass and infarct size from CMR imaging.[37] Beyhoff et al[38] showed that in isoproterenol-injected 129/Sv mice, echocardiographic GLS correlated well with the extent of subendocardial damages. Furthermore, GLS was ameliorated by mineralocorticoid receptor antagonists, accompanied by a reduction of cardiac fibrosis.[39] Strain analysis measured by echocardiography has been compared with CMR in small animals with mixed results. In models of genetic murine cardiomyopathy, global strain analysis from echocardiography was more variable and correlated only modestly with CMR parameters.[40] A limitation of our study is the relatively small number of animals investigated. However, we and others have previously demonstrated that in high-resolution CMR investigations, a smaller number of animals is sufficient to determine subtle (5–10%) changes in myocardial strain parameters.[12,35] Furthermore, we recently demonstrated in TAC mice that CMR-FT GCS and GLS are highly reproducible with excellent interobserver and intraobserver reproducibility, potentially being novel biomarkers for the detection of early myocardial dysfunction in small animal studies.[12]

Conclusions

The present study demonstrates that serelaxin significantly improves myocardial deformation parameters derived from quantitative CMR-FT as well as histomorphometric and gene expression findings in TAC mice. Using a comprehensive histology and biomarker analysis, we show in this study a correlation of morphological and functional parameters, demonstrating that CMR-FT is suitable to capture minute changes in regional myocardial performance and molecular biology in interventional studies.

Sources of Funding

The study was supported by a grant-in-aid from Novartis, Basel.

Disclosures

S.K., B.P., and P.S. were investigators in the RELAX-AHF-2 trial. P.S. received consultancy and lecture honoraria from Amgen, Novartis, Sanofi-Aventis, BMS/Pfizer, Daiichi-Sankyo, Bayer, BerlinChemie, and AstraZeneca. S.K. received an unrestricted research grant by Philips Healthcare and Myocardial Solutions. S.K. received speaker honoraria from Novartis, Berlin-Chemie, and AstraZeneca and was supported by DZHK (German Centre for Cardiovascular Research) and BMBF (German Ministry of Education and Research). B.P. reports having received consultancy and lecture honoraria from Bayer, Daiichi Sankyo, MSD, Novartis, Sanofi-Aventis, Stealth Peptides, and Vifor Pharma; and editor honoraria from the *Journal of the American College of Cardiology*. U.K. received research grants from Bayer; speaker honoraria from Bayer, BerlinChemie, Novartis, Sanofi-Aventis, and Servier; and participated in advisory boards of BerlinChemie, Boehringer Ingelheim, and Sanofi-Aventis. The remaining authors have no disclosures to report.

References

1. Benjamin EJ, Virani SS, Callaway CW, Chamberlain AM, Chang AR, Cheng S, Chiuve SE, Cushman M, Delling FN, Deo R, de Ferranti SD, Ferguson JF, Fornage M, Gillespie C, Isasi CR, Jimenez MC, Jordan LC, Judd SE, Lackland D, Lichtman JH, Lisabeth L, Liu S, Longenecker CT, Lutsey PL, Mackey JS, Matchar DB, Matsushita K, Mussolino ME, Nasir K, O'Flaherty M, Palaniappan LP, Pandey A, Pandey DK, Reeves MJ, Ritchey MD, Rodriguez CJ, Roth GA, Rosamond WD, Sampson UKA, Satou GM, Shah SH, Spartano NL, Tirschwell DL, Tsao CW, Voeks JH, Willey JZ, Wilkins JT, Wu JH, Alger HM, Wong SS, Muntner P; American Heart Association Council on Epidemiology and Prevention Statistics Committee and Stroke Statistics Subcommittee. Heart disease and stroke statistics—2018 update: a report from the American Heart Association. *Circulation*. 2018;137:e67–e492.
2. Gheorghiade M, Vaduganathan M, Fonarow GC, Bonow RO. Rehospitalization for heart failure: problems and perspectives. *J Am Coll Cardiol*. 2013;61:391–403.
3. Abebe TB, Gebreyohannes EA, Tefera YG, Abegaz TM. Patients with HFpEF and HFrEF have different clinical characteristics but similar prognosis: a retrospective cohort study. *BMC Cardiovasc Disord*. 2016;16:232.
4. MacDonald MR, Wee PP, Cao Y, Yang DM, Lee S, Tong KL, Leong KT. Comparison of characteristics and outcomes of heart failure patients with preserved versus reduced ejection fraction in a multiethnic Southeast Asian cohort. *Am J Cardiol*. 2016;118:1233–1238.
5. Gheorghiade M, Abraham WT, Albert NM, Greenberg BH, O'Connor CM, She L, Stough WG, Yancy CW, Young JB, Fonarow GC. Systolic blood pressure at admission, clinical characteristics, and outcomes in patients hospitalized with acute heart failure. *JAMA*. 2006;296:2217–2226.
6. Braunwald E. Heart failure. *JACC Heart Fail*. 2013;1:1–20.
7. Ponikowski P, Voors AA, Anker SD, Bueno H, Cleland JG, Coats AJ, Falk V, Gonzalez-Juanatey JR, Harjola VP, Jankowska EA, Jessup M, Linde C, Nihoyannopoulos P, Parissis JT, Pieske B, Riley JP, Rosano GM, Ruilope LM, Ruschitzka F, Rutten FH, van der Meer P. 2016 ESC guidelines for the diagnosis and treatment of acute and chronic heart failure: the Task Force for the diagnosis and treatment of acute and chronic heart failure of the European Society of Cardiology (ESC). Developed with the special contribution of the Heart Failure Association (HFA) of the ESC. *Eur J Heart Fail*. 2016;18:891–975.
8. Teerlink JR, Cotter G, Davison BA, Felker GM, Filippatos G, Greenberg BH, Ponikowski P, Unemori E, Voors AA, Adams KF Jr, Dorobantu MI, Grinfeld LR, Jondeau G, Marmor A, Masip J, Pang PS, Werdan K, Teichman SL, Trapani A, Bush CA, Saini R, Schumacher C, Severin TM, Metra M; RELAXin in Acute Heart Failure (RELAX-AHF) Investigators. Serelaxin, recombinant human relaxin-2, for treatment of acute heart failure (RELAX-AHF): a randomised, placebo-controlled trial. *Lancet*. 2013;381:29–39.
9. Metra M, Teerlink JR, Cotter G, Davison BA, Felker GM, Filippatos G, Greenberg BH, Pang PS, Ponikowski P, Voors AA, Adams KF, Anker SD, Arias-Mendoza A, Avendano P, Bacal F, Bohm M, Bortman G, Cleland JGF, Cohen-Solal A, Crespo-Leiro MG, Dorobantu M, Echeverria LE, Ferrari R, Goland S, Goncalvesova E, Goudev A, Kober L, Lema-Osores J, Levy PD, McDonald K, Manga P, Merkely B, Mueller C, Pieske B, Silva-Cardoso J, Spinar J, Squire I, Stepinska J, Van Mieghem W, von Lewinski D, Wikstrom G, Yilmaz MB, Hagner N, Holbro T, Hua TA, Sabarwal SV, Severin T, Szecsody P, Gimpelewicz C; RELAX-AHF-2 Committees Investigators. Effects of serelaxin in patients with acute heart failure. *N Engl J Med*. 2019;381:716–726.
10. Samuel CS, Summers RJ, Hewitson TD. Antifibrotic actions of serelaxin—new roles for an old player. *Trends Pharmacol Sci*. 2016;37:485–497.

11. Lekgabe ED, Kiriazis H, Zhao C, Xu Q, Moore XL, Su Y, Bathgate RA, Du XJ, Samuel CS. Relaxin reverses cardiac and renal fibrosis in spontaneously hypertensive rats. *Hypertension*. 2005;46:412–418.
12. Lapinskas T, Grune J, Zamani SM, Jeuthe S, Messroghli D, Gebker R, Meyborg H, Kintscher U, Zaliunas R, Pieske B, Stawowy P, Kelle S. Cardiovascular magnetic resonance feature tracking in small animals—a preliminary study on reproducibility and sample size calculation. *BMC Med Imaging*. 2017;17:51.
13. Devereux RB, Alonso DR, Lutas EM, Gottlieb GJ, Campo E, Sachs I, Reichek N. Echocardiographic assessment of left ventricular hypertrophy: comparison to necropsy findings. *Am J Cardiol*. 1986;57:450–458.
14. Stawowy P, Blaschke F, Pfautsch P, Goetze S, Lippek F, Wollert-Wulf B, Fleck E, Graf K. Increased myocardial expression of osteopontin in patients with advanced heart failure. *Eur J Heart Fail*. 2002;4:139–146.
15. Salatzki J, Foryst-Ludwig A, Bentele K, Blumrich A, Smeir E, Ban Z, Brix S, Grune J, Beyhoff N, Klopfleisch R, Dunst S, Surma MA, Klose C, Rothe M, Heinzel FR, Krannich A, Kershaw EE, Beule D, Schulze PC, Marx N, Kintscher U. Adipose tissue ATGL modifies the cardiac lipidome in pressure-overload-induced left ventricular failure. *PLoS Genet*. 2018;14:e1007171.
16. Faul F, Erdfelder E, Lang AG, Buchner A. G*power 3: a flexible statistical power analysis program for the social, behavioral, and biomedical sciences. *Behav Res Methods*. 2007;39:175–191.
17. Rockman HA, Ross RS, Harris AN, Knowlton KU, Steinhelper ME, Field LJ, Ross J Jr, Chien KR. Segregation of atrial-specific and inducible expression of an atrial natriuretic factor transgene in an in vivo murine model of cardiac hypertrophy. *Proc Natl Acad Sci USA*. 1991;88:8277–8281.
18. Chien KR, Knowlton KU, Zhu H, Chien S. Regulation of cardiac gene expression during myocardial growth and hypertrophy: molecular studies of an adaptive physiologic response. *FASEB J*. 1991;5:3037–3046.
19. van den Bosch BJ, Lindsey PJ, van den Burg CM, van der Vlies SA, Lips DJ, van der Vusse GJ, Ayoubi TA, Doevendans PA, Smeets HJ. Early and transient gene expression changes in pressure overload-induced cardiac hypertrophy in mice. *Genomics*. 2006;88:480–488.
20. Travers JG, Kamal FA, Robbins J, Yutzey KE, Blaxall BC. Cardiac fibrosis: the fibroblast awakens. *Circ Res*. 2016;118:1021–1040.
21. Brew K, Nagase H. The tissue inhibitors of metalloproteinases (TIMPS): an ancient family with structural and functional diversity. *Biochem Biophys Acta*. 2010;1803:55–71.
22. Samuel CS, Unemori EN, Mookerjee I, Bathgate RA, Layfield SL, Mak J, Tregear GW, Du XJ. Relaxin modulates cardiac fibroblast proliferation, differentiation, and collagen production and reverses cardiac fibrosis in vivo. *Endocrinology*. 2004;145:4125–4133.
23. Wu XP, Wang HJ, Wang YL, Shen HR, Tan YZ. Serelaxin inhibits differentiation and fibrotic behaviors of cardiac fibroblasts by suppressing ALK-5/Smad2/3 signaling pathway. *Exp Cell Res*. 2018;362:17–27.
24. McCarthy JC, Aronovitz M, DuPont JJ, Calamaras TD, Jaffe IZ, Blanton RM. Short-term administration of serelaxin produces predominantly vascular benefits in the angiotensin II/L-NAME chronic heart failure model. *JACC Basic Transl Sci*. 2017;2:285–296.
25. Wang D, Luo Y, Myakala K, Orlicky DJ, Dobrinskikh E, Wang X, Levi M. Serelaxin improves cardiac and renal function in DOCA-salt hypertensive rats. *Sci Rep*. 2017;7:9793.
26. Giam B, Chu PY, Kuruppu S, Smith AI, Horlock D, Murali A, Kiriazis H, Du XJ, Kaye DM, Rajapakse NW. Serelaxin attenuates renal inflammation and fibrosis in a mouse model of dilated cardiomyopathy. *Exp Physiol*. 2018;103:1593–1602.
27. Celutkiene J, Plymen CM, Flachskampf FA, de Boer RA, Grapsa J, Manka R, Anderson L, Garbi M, Barberis V, Filardi PP, Gargiulo P, Zamorano JL, Lainscak M, Seferovic P, Ruschitzka F, Rosano GM, Nihoyannopoulos P. Innovative imaging methods in heart failure: a shifting paradigm in cardiac assessment. Position statement on behalf of the Heart Failure Association of the European Society of Cardiology. *Eur J Heart Fail*. 2018;20:1615–1633.
28. Shah AM, Solomon SD. Myocardial deformation imaging: current status and future directions. *Circulation*. 2012;125:e244–e248.
29. Cho GY, Marwick TH, Kim HS, Kim MK, Hong KS, Oh DJ. Global 2-dimensional strain as a new prognosticator in patients with heart failure. *J Am Coll Cardiol*. 2009;54:618–624.
30. Nahum J, Bensaid A, Dussault C, Macron L, Clemence D, Bouhemad B, Monin JL, Rande JL, Gueret P, Lim P. Impact of longitudinal myocardial deformation on the prognosis of chronic heart failure patients. *Circ Cardiovasc Imaging*. 2010;3:249–256.
31. Buss SJ, Breuninger K, Lehrke S, Voss A, Galuschky C, Lossnitzer D, Andre F, Ehlermann P, Franke J, Taeger T, Frankenstein L, Steen H, Meder B, Giannitsis E, Katus HA, Korosoglou G. Assessment of myocardial deformation with cardiac magnetic resonance strain imaging improves risk stratification in patients with dilated cardiomyopathy. *Eur Heart J Cardiovasc Imaging*. 2015;16:307–315.
32. Mahfoud F, Urban D, Teller D, Linz D, Stawowy P, Hassel JH, Fries P, Dreysse S, Wellnhofer E, Schneider G, Buecker A, Schneeweis C, Doltra A, Schlaich MP, Esler MD, Fleck E, Bohm M, Kelle S. Effect of renal denervation on left ventricular mass and function in patients with resistant hypertension: data from a multi-centre cardiovascular magnetic resonance imaging trial. *Eur Heart J*. 2014;35:2224–2231b.
33. Bernard A, Donal E, Leclercq C, Schnell F, Fournet M, Reynaud A, Thebault C, Mabo P, Daubert JC, Hernandez A. Impact of cardiac resynchronization therapy on left ventricular mechanics: understanding the response through a new quantitative approach based on longitudinal strain integrals. *J Am Soc Echocardiogr*. 2015;28:700–708.
34. Lindsey ML, Kassiri Z, Virag JA, de Castro Bras LE, Scherrer-Crosbie M. Guidelines for measuring cardiac physiology in mice. *Am J Physiol Heart Circ Physiol*. 2018;314:H733–H752.
35. van Nierop BJ, van Assen HC, van Deel ED, Niesen LB, Duncker DJ, Strijkers GJ, Nicolay K. Phenotyping of left and right ventricular function in mouse models of compensated hypertrophy and heart failure with cardiac MRI. *PLoS One*. 2013;8:e55424.
36. Furihata T, Kinugawa S, Takada S, Fukushima A, Takahashi M, Homma T, Masaki Y, Tsuda M, Matsumoto J, Mizushima W, Matsushima S, Yokota T, Tsutsui H. The experimental model of transition from compensated cardiac hypertrophy to failure created by transverse aortic constriction in mice. *Int J Cardiol Heart Vasc*. 2016;11:24–28.
37. Bhan A, Sirker A, Zhang J, Protti A, Catibog N, Driver W, Botnar R, Monaghan MJ, Shah AM. High-frequency speckle tracking echocardiography in the assessment of left ventricular function and remodeling after murine myocardial infarction. *Am J Physiol Heart Circ Physiol*. 2014;306:H1371–H1383.
38. Beyhoff N, Brix S, Betz IR, Klopfleisch R, Foryst-Ludwig A, Krannich A, Stawowy P, Knebel F, Grune J, Kintscher U. Application of speckle-tracking echocardiography in an experimental model of isolated subendocardial damage. *J Am Soc Echocardiogr*. 2017;30:1239–1250.e1232.
39. Grune J, Beyhoff N, Smeir E, Chudek R, Blumrich A, Ban Z, Brix S, Betz IR, Schupp M, Foryst-Ludwig A, Klopfleisch R, Stawowy P, Houtman R, Kolkhof P, Kintscher U. Selective mineralocorticoid receptor cofactor modulation as molecular basis for finerenone's antifibrotic activity. *Hypertension*. 2018;71:599–608.
40. Azam S, Desjardins CL, Schluchter M, Liner A, Stelzer JE, Yu X, Hoit BD. Comparison of velocity vector imaging echocardiography with magnetic resonance imaging in mouse models of cardiomyopathy. *Circ Cardiovasc Imaging*. 2012;5:776–781.